COMBINED TRANSPORT AND STATISTICAL DESCRIPTION OF HEAVY-ION FRAGMENTATION REACTIONS*

T.I. Mikhailova[a], B. Erdemchimeg[a,b], A.G. Artukh[a]
M. Di Toro[c], H.H. Wolter[d]

[a]JINR, Dubna, Russia
[b]Mongolian National University, Ulaanbaatar, Mongolia
[c]LNS-INFN, Catania, Italy
[d]University of Munich, Munich, Germany

(Received December 21, 2018)

We summarize a description of heavy-ion fragmentation reactions at low and intermediate energies in terms of a Boltzmann–Vlasov transport approach for the production of the hot, excited primary fragments, followed by a statistical decay of these to arrive at the measured cold fragments. We compare isotope distributions and velocity spectra to experimental data. While the isotopic distributions are reasonably well-described by this microscopic approach, there are larger differences in the velocity distributions. These seem to be due to too small fluctuations in the transport calculation and to the presence of more direct reaction processes in the data.

DOI:10.5506/APhysPolBSupp.12.619

1. Introduction

The final state of heavy-ion collisions with energies between the Fermi energy and a few hundred MeV per nucleon consists not mainly of free nucleons, but of a large number of light clusters ($A \leq 4$) and also of a substantial number of intermediate mass fragments (IMF). This nuclear fragmentation is seen as a consequence of a liquid-gas transition in the phase diagram of nuclear matter. Fragments yields are important for the production of exotic nuclear beams and for many applications in technology and medicine. Therefore, it is of interest to understand the mechanism of fragmentation, and the appropriate way to describe it theoretically. There are several successful empirical methods [1], but a more microscopic model is desirable. In

* Presented at the XXV Nuclear Physics Workshop "Structure and Dynamics of Atomic Nuclei", Kazimierz Dolny, Poland, September 25–30, 2018.

this contribution, we discuss a two-stage approach: the first step is to apply transport theory to describe the non-equilibrium dynamics of the violent interaction between the colliding nuclei. This results in "primary" fragments, defined as the fragments which exist when the strong interaction between them becomes negligible. The primary fragments are still highly excited. The second step is then the de-excitation by nucleon and fragment emission as a statistical process, which is described here by a statistical fragmentation model.

Qualitatively, a reaction in this energy range can be well-characterized by a so-called Wilczyński diagram [2], which plots the yield as a function of the total kinetic energy loss of the projectile in the center of mass and the deflection angle of the residual primary projectile fragment. Examples for reactions of light heavy ions on a heavy Ta target at energies between 35 and 140 A MeV are shown in Fig. 1. The O+Ta reaction at the lowest energy shows the typical orbiting behaviour of deep-inelastic processes. The negative deflection angles result in longer contact and thus larger energy loss, *i.e.* more friction. At the much higher energy of the Ca+Ta reaction at 140 A MeV, the process is more of the abrasion–ablation-type. The projectile remnant moves essentially in the forward direction, but with closer impact parameter more nucleons and energy are lost to the target. A microscopic description will have to be able to describe this evolution of the process with energy without adjusting parameters.

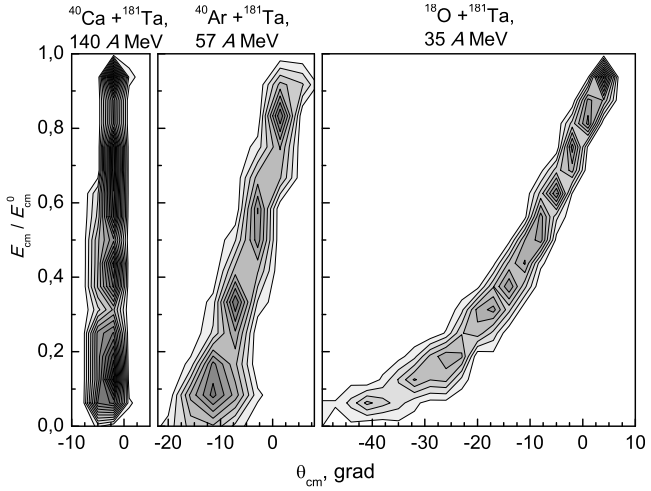

Fig. 1. The Wilczyński contour plot of the logarithm of the yield as a function of the ratio of the final and initial kinetic energies of the projectile in the cm and of the deflection angle. The contour plot shows the yields of the residual fragment obtained from transport calculations [3–5].

2. Theoretical considerations

Here, we use a transport approach to heavy-ion collisions in terms of the one-body phase-space distribution function $f(\vec{r},\vec{p},t)$. The Boltzmann–Nordheim–Vlasov (BNV) transport approach, often also called the Boltzmann–Uehling–Uhlenbeck (BUU) approach, describes the time evolution of the distribution function under the influence of a self-consistent mean field $U([f])$ and a two-body collision term, which includes the effect of Pauli blocking [6]

$$\frac{\partial f_1}{\partial t}+\frac{\vec{p}_1}{m}\nabla_{\vec{r}}f_1-\nabla_{\vec{r}}U\nabla_{\vec{p}_1}f_1=\left(\frac{2\pi}{m}\right)^3\int \mathrm{d}\vec{p}_2\mathrm{d}\vec{p}_3\mathrm{d}\vec{p}_4|\vec{v}_1-\vec{v}_2| \\ \times\sigma_{NN}(\Omega_{12})\delta\left(\vec{p}_1+\vec{p}_2-\vec{p}_3-\vec{p}_4\right)\left(f_3f_4\bar{f}_1\bar{f}_2-f_1f_2\bar{f}_3\bar{f}_4\right)\,. \tag{1}$$

Here, $f_i=f(\vec{r},\vec{p}_i,t)$, $\bar{f}_i=(1-f_i)$ is the Pauli blocking factor for the final state of the collision, $v_i=p_i/m$ are velocities, $\sigma_{NN}(\Omega)$ is the in-medium NN cross section. The two terms in the collision integral are the gain and loss terms due to 2-body collisions. This non-linear equation is solved by simulations using the test particles (TP) method, which is described, *e.g.* in Ref. [6]. The collision term is simulated stochastically, by performing test particle collisions with a probability depending on the cross section and checking the Pauli principle for the final state. The potential $U([f])$ and the cross section are either derived from an energy density functional, or parametrized in order to test them relative to the data (here, a Skyrme functional and parametrized cross sections are used [3, 7]). There is an alternative transport approach, called Quantum Molecular Dynamics (QMD), which describes the evolution in terms of nucleon coordinates and momenta [8]. We do not go into the details of this method here.

The colliding nuclei are initialized by distributing TPs stochastically to reproduce a given density distribution, which here is taken as a Fermi function reproducing the experimentally determined radius and diffuseness. The momenta are chosen stochastically from the local Fermi sphere depending on the local density. Using our energy density functional, we calculate the binding energy of our constructed initial nuclei. In Fig. 2, these are compared for some elements and sequences of isotopes to the ground state energies from a standard liquid-drop formula with parameters taken from Ref. [9]. The calculations follow in general the trend of the realistic energies, but in detail they are not exact, which is due to the rather rough construction of the ground state. In fact, these nuclei are not very stable when propagated freely with the transport code, as was shown *e.g.* in Ref. [5]. They evaporate nucleons and change the intrinsic energy. A better construction of the initial nuclei would be desirable, *e.g.* with using the semi-classical Thomas–Fermi theory. This is presently in progress.

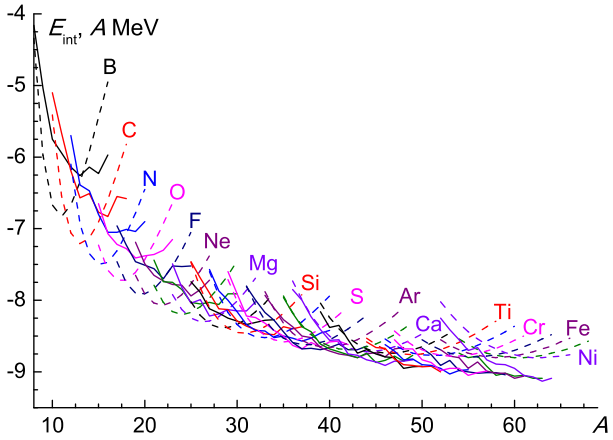

Fig. 2. Binding energies for isotopic chains for some elements identified by symbols. Compared are the results of the intialized nuclei in our treatment (solid lines, see the text) with the results of a liquid-drop formula (dashed lines).

Fragments are identified with a coalescence criterion in coordinate and momentum space at the so-called freeze-out time when the different fragments are sufficiently isolated so that nuclear forces between them become negligible. These are the "primary" or "hot" fragments, since they are still excited by 3–4 A MeV for central collisions and decreasing with impact parameter. The excitation energy is determined by comparing to the energy of a freely propagated fragment with the same N and Z. While, as discussed above, these energies are only approximate, the differences between the primary fragment and the corresponding ground state is expected to be more realistic. The de-excitation of the primary fragment is important when comparing to experiments which measure the final cold fragments. It cannot be described by the transport approach for two reasons: firstly, as seen above, the transport description is not reliable for longer time scales. Secondly, the detailed pathway of de-excitation depends on quantum structures in the excited nuclei, which are not contained in the semi-classical description of the nuclei and fragments. We, therefore, employ a statistical model to describe the de-excitation and cooling of the primary fragments, namely the widely-used Statistical Multifragmentation Model (SMM) [10], where we consider evaporation, Fermi break-up, and multifragmentation modes. The primary fragments are propagated from freeze-out time to infinity analytically by the Coulomb interaction between projectile- and target-like fragments. Then the de-excitation is calculated, to obtain the cold final fragments and their kinetic energies.

3. Results

We consider reactions which cover a range of incident energies from 35 to 140 A MeV per nucleon and a variety of projectiles always on the same target ^{181}Ta. The projectiles and bombarding energies are ^{18}O at 35 A MeV [3, 11]; ^{40}Ar at 57 A MeV [4, 12]; ^{40,48}Ca at 140 A MeV [5, 13], and ^{64}Ni at 140 A MeV [13, 14]. Here the references [11–13] refer to the data, and the references [3–5, 14] to our previous analyses of them, respectively.

We will first discuss the results in detail for a representative example: ^{40}Ar on ^{181}Ta at 57 A MeV [4, 12]. In Fig. 3, we show the yield distribution of the fragments as contour plots in the N–Z plane from 50 BNV runs integrated over the impact parameter, limited to the experimental acceptance angle of $\pm$ 5 degrees in the lab. The left panel shows the primary fragments from the transport calculation at freeze-out time. The rather narrow distribution ranges from fragments near the projectile ($Z = 18, N = 22$) to light fragments around $Z = 5$ with two components. As seen from Fig. 1 (middle panel), inside the acceptance angles, it has a component for nuclei near the projectile, and one for large energy losses, where the distribution in deflection angle becomes wide. The middle panel is the distribution after the application of the statistical code. Now, the distribution covers the whole range of fragments from the projectile to light clusters and is considerably wider. The rightmost panel shows the experimental results from

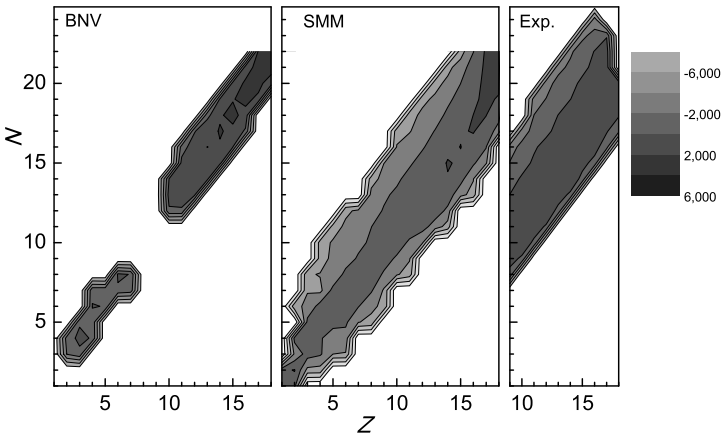

Fig. 3. Contour plots of yield of fragments (logarithmic scale) in the N–Z plane from a ^{40}Ar on ^{181}Ta collision at 57 A MeV. The panels show from left to right: the distribution of primary ("hot") fragments at freeze-out time, the distribution after applying the statistical decay model SMM, and the distribution for the available experimental data from Ref. [12].

Ref. [12], which were only obtained for elements of $Z \geq 8$. It is seen that the population after decay bears a much greater similarity to the data than the hot population, which shows the importance of considering transport and statistical decay together.

A more quantitative representation of the results is given in Fig. 4, where we show in the left panel the cross section for sulphur isotope production for the hot primary fragments (BNV), the cold fragments (BNV+SMM) and the experiment. Thus, these isotope distributions are a cut through the contour plots of Fig. 3 at $Z = 16$. It is seen how the isotope distribution after de-excitation shifts to lower elements and becomes wider. It is then rather similar to the experimental distribution.

The right panel of Fig. 4 shows the velocity distribution as a function of reduced velocity (normalized to the initial projectile velocity) for hot and cold calculated and for experimental sulphur fragments summed over the isotopes. Comparing the hot and the cold distribution, there is a broadening and a shift of the distribution. The statistical decay is isotropic and will thus broaden the distribution, which is not a very big effect in this case. Since the fragment also loses kinetic energy, there should be a shift to lower velocities. However, with the emission of charged particles, there is a contribution from heavier primary fragment elements, which have higher velocities. Thus, there is a competition between these effects, which in this case slightly increases the average position of the distribution. In comparison

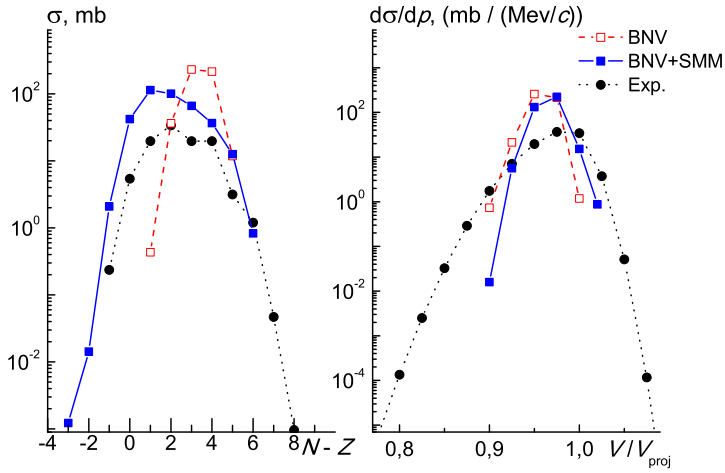

Fig. 4. Results for the reaction of ^{40}Ar on ^{181}Ta at 57 A MeV. Isotope distributions for the element S (left panel); velocity distributions for S summed over isotopes (right panel). In each case, we show the distribution of the hot fragments (BNV, open square, dashed line), the cold fragments (BNV+SMM, solid square, solid line), and the experiment (solid circle, dotted line) [12].

to experiment, this effect, however, is not enough; the experimental distribution has higher average velocity and is much wider. The width of the calculated distribution depends on the fluctuations in the transport calculations. This is an interesting and much discussed question, which we cannot treat in detail here [15]. It appears that the fluctuations in this method of calculation are not large enough.

However, there is another source of the width of the experimental distributions. It is observed that these reach velocities greater than the initial velocity. The BNV distributions as a dissipative dynamics cannot have velocities greater than the initial velocity. Due to the stochastic decay, velocities can be slightly enlarged, but not enough relative to the data. While the calculated hot and cold fragments have roughly a Gaussian form, the data have an asymmetric distribution, and have often been fitted with two half-Gaussians with different widths [12]. The possible interpretation is that the data contain two components, a "direct" one centred around beam velocity and a dissipative one at smaller velocities. The calculations only describe the dissipative component. The direct component has been associated with more direct reaction mechanisms, like break-up or multi-nucleon transfer. The treatment of such a component in the transport descriptions is an open question.

For a better comparison, one may attempt to extract the dissipative component from the data. In the fit with two half-Gaussians, the right half (*i.e.* for reduced velocities larger than unity) should be due to direct processes. The full right-hand Gaussian can thus be subtracted from the data to approximately obtain the dissipative component. An example of this will be seen below.

In Fig. 5, we show isotope distributions for the five reactions, given in the beginning of this section and identified in each row to the right. For each reaction, the distributions are given for the projectile and for elements one or two charges below. Shown are the distributions for the hot (BNV), cold (BNV+SMM), and experimental data. It is seen as a general behaviour that the hot fragment distribution is narrow and the neutron richness is like that of the projectile, which points to an abrasion-like process. In the de-excitation, predominantly neutrons are emitted, and the distribution moves in the direction of more symmetry. This shift, therefore, is not very strong for the symmetric projectiles ^{16}O and ^{40}Ca. Generally, one can say that the description of the data is reasonable, considering that no parameters of the calculation are adjusted to the reaction.

Finally, in Fig. 6, we show velocity distributions for the same reactions and elements as in Fig. 5, summed over the isotopes. Similar effects are seen as in the example of ^{40}Ar+Ta, discussed above in Fig. 4. The primary distributions are rather narrow. Including the statistical decay, the widths are

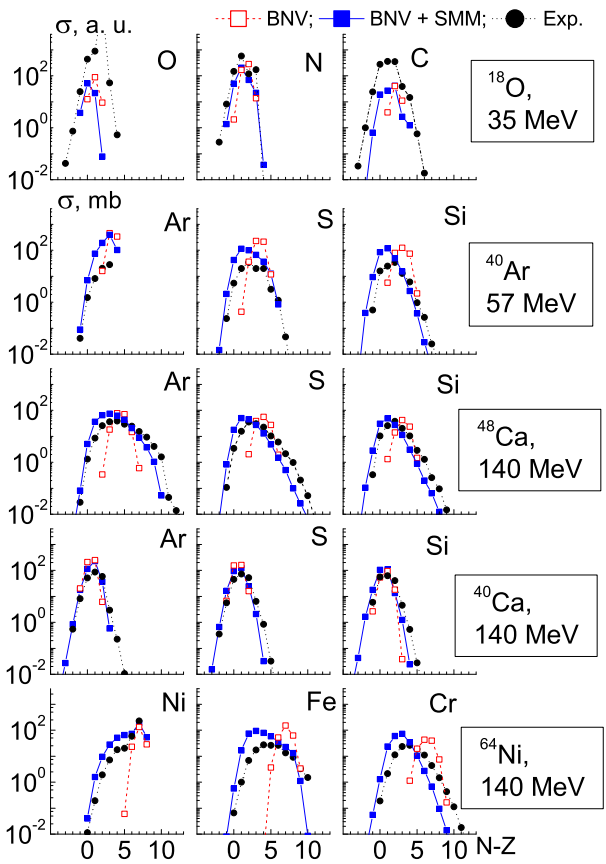

Fig. 5. (Color online) Isotope distributions for different reactions on the target ^{181}Ta. The projectile and the incident energy are identified in each row at the right. For each reaction, we give the isotope distribution for three elements identified in the upper corner of each panel. The lines are: BNV (open square, dashed line, red), BNV+SMM (solid square, solid line, blue), experiment (solid circle, dotted line, black).

somewhat increased, and the distributions become more comparable to the data. The de-excitation shifts the distribution sometimes to higher, sometimes to lower velocities due to the competition mentioned above between energy loss and contributions from higher elements. The widths are generally substantially smaller than the experimental widths. As noted above, this may be due to not enough fluctuations in the calculation, but also to a direct component in the experimental data, which is not included in the transport approach. This is shown in the figure more explicitly in the case of the O+Ta reaction, where the dissipative experimental contribution has been extracted as discussed above (open circles). This improves the fit to

the data on the higher velocity side. It is seen that the discrepancies with experiment reduce with higher projectile energies, since the direct component is expected to decrease with energy.

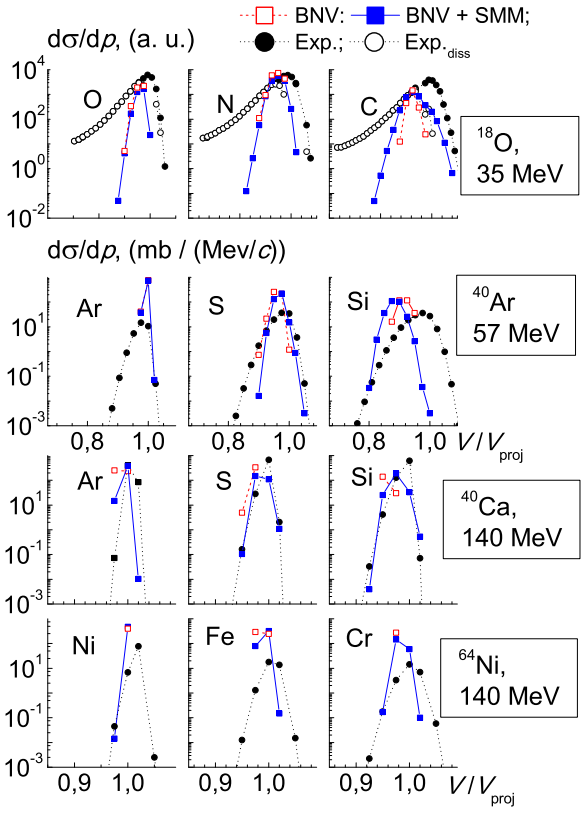

Fig. 6. Velocity distributions for the same reactions and fragments as in Fig. 5 plotted against the reduced velocity. The signatures of the lines are identified in the legend and are the same as in Fig. 5.

4. Summary and conclusion

We have discussed a microscopic description of heavy-ion fragmentation reactions, which contains a transport description for the violent interaction between the nuclei and a statistical description of the decay of the excited primary fragments. It is evident that both ingredients are important for a satisfactory description of the different aspects of these reactions. The method has been applied to various light heavy-ion reactions at energies from the deep-inelastic to the intermediate-energy regime. The input is obtained from the literature and is not adjusted to the data.

The isotope distributions are reproduced reasonably, while there are bigger discrepancies in the velocity or energy spectra of the emitted fragments. Especially, the width of the spectra is sensitive to the model description and the contributing processes. The too small width of the calculations points to too small fluctuation in the transport description, but also indicates that other reaction processes may be present, which are not captured by the dissipative dynamics of the transport theory. Thus, velocity distributions contain additional information about the mechanism of the reaction. Generally, however, the method is well-suited to estimate the fragment production in heavy-ion collisions, considering that it does not use any adjusted parameters.

The authors thank A. Botvina for providing us the computer code SMM and for useful advice. This work was supported by the Heisenberg–Landau Program. T.M. was supported by the Russian Foundation for Basic Research under grant No. 17-01-00661-a, and HHW by the Universe Cluster of Excellence of the DFG Germany.

REFERENCES

[1] K. Sümmerer, *Phys. Rev. C* **86**, 014601 (2012); D. Lacroix *et al.*, *Phys. Rev. C* **69**, 054604 (2004); A.S. Goldhaber, *Phys. Lett. B* **53**, 306 (1974); M. Veselsky *et al.*, *Nucl. Phys. A* **781**, 521 (2007).

[2] J. Wilczyński, *Phys. Lett. B* **47**, 484 (1973).

[3] T.I. Mikhailova *et al.*, *Phys. Part. Nucl. Lett.* **12**, 409 (2015).

[4] T.I. Mikhailova *et al.*, *Bull. Russ. Acad. Sci. Phys* **78**, 1131 (2014).

[5] T.I. Mikhailova *et al.*, *Phys. Atom. Nucl.* **79**, 604 (2016); *Acta Phys. Pol. B Proc. Suppl.* **10**, 121 (2017).

[6] G.F. Bertsch, S. Das Gupta, *Phys. Rep.* **160**, 189 (1988).

[7] V. Baran, M. Colonna, V. Greco, M. Di Toro, *Phys. Rep.* **410**, 335 (2005).

[8] J. Aichelin, *Phys. Rep.* **202**, 233 (1991).

[9] C. Bertulani, P. Danielewicz, *Introduction to Nuclear Reactions*, Institute of Physics Publishing, Graduate Students Series in Physics, 2004.

[10] J.P. Bondorf *et al.*, *Phys. Rep.* **257**, 133 (1995); A. Ergun *et al.*, *Phys. Rev. C* **92**, 014610 (2015).

[11] A.G. Artukh *et al.*, *Nucl. Phys. A* **701**, 96c (2002).

[12] X.H. Zhang *et al.*, *Phys. Rev. C* **85**, 024621 (2012).

[13] M. Mocko *et al.*, *Phys. Rev. C* **74**, 054612 (2006); M. Mocko *et al.*, *Phys. Rev. C* **78**, 024612 (2008).

[14] T.I. Mikhailova *et al.*, *EPJ Web Conf.* **173**, 04010 (2018).

[15] M. Colonna *et al.*, *Phys. Rev. C* **82**, 054613 (2010).